Few-femtosecond $C_2H_4^+$ internal relaxation dynamics accessed by selective excitation

Matteo Lucchini,[*,†,‡] Benoit Mignolet,[¶] Mario Murari,[†,‡] Cayo E. M. Gonçalves,[¶] Giacinto D. Lucarelli,[†] Fabio Frassetto,[§] Luca Poletto,[§] Françoise Remacle,[¶] and Mauro Nisoli[†,‡]

†*Department of Physics, Politecnico di Milano, 20133 Milano, Italy*
‡*Institute for Photonics and Nanotechnologies, IFN-CNR, 20133 Milano, Italy*
¶*Theoretical Physical Chemistry, UR MOLSYS, University of Liège, B4000 Liège, Belgium*
§*Institute for Photonics and Nanotechnologies, IFN-CNR, 35131 Padova, Italy*

E-mail: matteo.lucchini@polimi.it

Abstract

Dissociation of ethylene cation is a prototypical multistep pathway in which the exact mechanisms leading to internal energy conversions are not fully known. In the last years, theoretical investigations have proposed different explanations which are often not completely compatible. For this reason, it is still unclear how the energy is exactly redistributed among the internal modes and which step is rate determining. Here we use few-fs extreme-ultraviolet (EUV) pulses of tunable energy to selectively excite the four lowest cationic states of $C_2H_4^+$ and probe the subsequent fast relaxation with a short IR pulse. Our results demonstrate that the delayed IR pulse photoexcites the cationic ground state (GS) to higher excited states, producing a hot GS upon relaxation, which enhances the fragmentation yield. As the photoexcitation probability of the GS strongly depends on the molecular geometry, the delayed probing by the IR pulse provides information about the ultrafast excited state dynamics such as the type of conical intersection (planar or twisted) involved in the nonradiative relaxation in the first 20 fs.

TOC Graphic

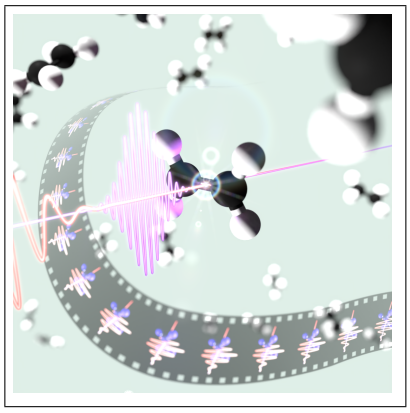

The photochemistry of many molecular systems is defined by the ultrafast dynamics which unfold in the first femtoseconds after optical excitation.[1] The investigation of these dynamics is not trivial, both experimentally and theoretically. From the experimental point of view, it requires few-femtosecond light pulses.[2,3] Theoretically, the full brute-force description of a many-body system becomes impractical already at the atomic level, when more than two electrons are present. As a result, most of ultrafast dynamics initiated by light pulses remain unexplored despite their importance. A remarkable example is the relaxation dynamics of the simplest π-radical system:[4] ethylene cation $C_2H_4^+$. Its dissociation is a typical multi-step pathway[5–7] in which the exact mechanisms leading to internal energy conversions are not fully known[8–10] and recent theoretical investigations proposed different mechanisms which are not completely compatible to one another.[8,11] For this reason, it is still unclear how the energy is redistributed among the internal modes and which step is rate determining. In this Letter we have used 15-fs EUV femtosecond pulses in combination with short (15 fs) and intense infrared (IR) pulses to study the ultrafast molecular relaxation in a pump-probe scheme. EUV pulses of tunable photon energy are used to create a coherent superposition of the four lowest $C_2H_4^+$ states and initiate relaxation dynamics which eventually lead to molecular fragmentation. The IR pulse further photoexcites the molecule leading to the formation of a hot ground state,[12] which then enhances the fragmentation yield. The photoexcitation strongly depends on the initial states accessed by the EUV pulse and on the EUV-IR pulse delay. Excited state dynamical simulations with surface hopping[13] allowed us to identify the IR excitation mechanism as 3-photon absorption process which takes place mainly on the cationic ground state, D0, and maximizes only for particular molecular geometries (see Fig. 1(a)). This proves the dynamics observed in the final fragmentation yield to be sensitive to the actual population on D0. As a consequence the timing of the $C_2H_4^+$ pump-probe signal directly interviews the overall relaxation process, shedding new light onto the role of subsequent IR excitation and opening new routes towards the manipulation and control of complex relaxation processes in organic molecules with few-femtosecond pulses.

Figure 1(b) reports a scheme of the experimental setup. IR pulses with a duration of 15 fs, central wavelength of about 811 nm and peak intensity $I_{IR} = 3.3 \times 10^{12}\,\mathrm{W/cm^2}$, are focused onto a Xe gas target to obtain EUV light through high-order harmonic generation (HHG).[2] The harmonic radiation is then sent into a time-delay compensated monochromator (TDCM),[14] which consists of two sections working in a subtractive configuration to compensate for the temporal and spectral dispersion. As a result, it is possible to select a single harmonic, while preserving its original temporal characteristics.[15] After selection, the EUV radiation is focused on an ethylene gas target placed in the focal spot of a time-of-flight (TOF) mass spectrometer. An EUV spectrometer at the end of the setup is used to inspect the harmonic spectra.

Here we used the TDCM to select the 9^{th}, the 11^{th} and the 13^{th} harmonic of the fundamental (hereafter H9, H11 and H13) whose spectra are reported in Fig. 1(c). The time duration of each harmonic has been characterized by photoelecron cross-correlation measurements[18] (see SI). We found H9 to last for 15 ± 2.2 fs, while H11 and H13 have a duration of 11 ± 1.8 fs and 7.7 ± 2.4 fs, respectively. Since the three harmonics have photon energy comparable with the vertical transitions from the C_2H_4 ground state to the lowest excited states of the molecular cation (black horizontal marks in Fig. 1(c)), it is possible to control the initial superposition of molecular states after ionization by changing the selected harmonic. Figure 1(d) shows the initial state population evaluated by multiplying the experimental cross-section reported in Ref.[4] with the harmonic spectra of Fig. 1(c). As it is possible to notice, H9 enables a very efficient excitation of the cationic ground state $\tilde{\mathrm{X}}$, H11 of the first excited state $\tilde{\mathrm{A}}$, while H13 predominantly excite the $\tilde{\mathrm{B}}$ and $\tilde{\mathrm{C}}$ states. Figure 1(e) shows the photoelectron spectra associated with C_2H_4 ionization by the three harmon-

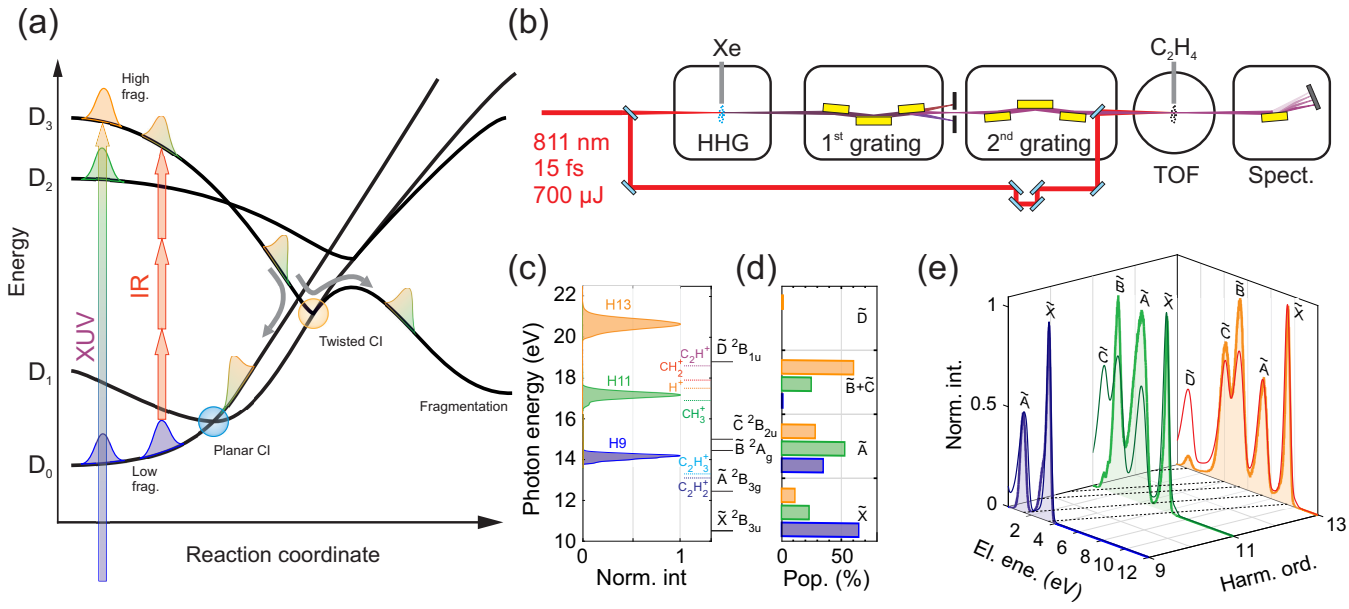

Figure 1: **(a)** Relaxation scheme: the EUV radiation projects the wave-packet onto the four lowest cationic states. The population of the excited states quickly relaxes to the ground state through planar and twisted conical intersections, ultimately leading to fragmentation. The higher the initial excitation the more fragments are produced (see Fig. 2(a)). Once relaxed onto the ground state, the molecule can be re-excited by the IR field via three-photon absorption, thus triggering further relaxation and fragmentation. **(b)** Schematic of the experimental setup composed by the EUV source (high-order harmonic generation, HHG), a time-delay compensated monochromator (TDCM), a TOF spectrometer and an XUV spectrometer. **(c)** Spectrum of the three harmonics together with the vertical transition energies (black horizontal lines) and the fragment appearance potentials (colored dotted lines).[16] **(d)** Initial state populations calculated with the partial cross-sections taken from[4] and the harmonic spectra in (c). **(e)** Photoelectron spectra obtained by ionizing C_2H_4 with the harmonics in (c) (same color code). The thinner curves represent the convolution between the high-resolution spectrum from[17] and the actual harmonic spectra.

ics. The experimental data qualitatively follow the convolution of the high-resolution spectra reported by Holland et al.[17] with the actual harmonic spectra (Fig. 1(c)), hence confirming that the molecular cation is prepared in different initial states as reported in Fig. 1(d).

As the internal relaxation process following photoexcitation by a selected harmonic can eventually lead to molecular fragmentation, a complementary approach is to study the positive fragments which are created after ionization. Figure 2(a) shows the main ions produced with the EUV pulses (the complete fragmentation spectra are reported in the SI). As a consequence of the selective excitation, the fragment yield pertaining to different harmonics qualitatively differ from each other. In particular, ionization by H9 presents a clear reduced production of the $C_2H_3^+$ and $C_2H_2^+$ fragments, which are related to the process of H and H_2 loss, respectively. Furthermore, in contrast to what happens with H11 and H13, there is a clear suppression of H loss with the H_2 loss process becoming favored (Fig. 2(b)). An increasing H/H_2 loss in ethylene cation with increasing excitation energy has already been observed and discussed in the literature, yet its exact origin remains unclear and substantially different explanations have been proposed.[8,11] To investigate the underling relaxation dynamics we followed a pump-probe scheme and further excite the molecule with the IR pulse. Figures 2(c)-(e) show the differential ion yield, defined as the difference between the ion yield obtained with

and without the IR pulse divided by the latter: $\Delta Y(\tau) = (Y_{IR}(\tau) - Y_0)/Y_0$, for the first three heaviest fragments and as a function of the delay, τ, between the EUV and IR pulses.

In all figures, the markers represent the average over 10 independent pump-probe measurements, while the error bars cover twice their standard deviation. Within a single scan, a mechanical shutter allows to acquire an EUV-only reference signal each two laser shots for efficient noise removal. Before and after each set of scans we perform a photoelectron pump-probe experiment which has a two-fold purpose: (*i*) to extract the EUV-IR cross-correlation signal and monitor the temporal characteristics of the pulses (see SI), (*ii*) to precisely identify the temporal overlap between the pulses and eventually monitor any mechanical drift of the pump-probe interferometer. Within the accessible range we found the observed features to be largely independent of the IR probe intensity (see SI).

The results obtained with H13 (orange curve) and H11 (green curve) are qualitatively similar. At the pump-probe overlap the additional energy deposited by the IR pulse favors the production of small fragments (see SI), partially bleaching the $C_2H_3^+$ and $C_2H_2^+$ yield (Figs. 2(d),(e)), but without any evident effect on the molecular cation signal (Fig. 2(c)). At a delay of about 20 fs, instead, the molecular cation signal reduces and correlates to further H and H_2 loss which increase the $C_2H_3^+$ and $C_2H_2^+$ yield. The results obtained with H9 are qualitatively different (blue curves and markers). The $C_2H_4^+$ bleaching is now broader and maximum directly at the pump probe overlap. The $C_2H_3^+$ and $C_2H_2^+$ relative yield exhibits a considerably slower and stronger variation. This latter could be explained as follows: ionization by an H9 photon leads to a lower production of $C_2H_3^+$ and $C_2H_2^+$ if compared to H11 and H13 photons (see Figs. 2(a),(b)). Nevertheless, for the molecule ionized with the H9 harmonic the absorption of several IR photons provides extra energy, which may enhance the fragmentation yield.

In the following we will concentrate on the different timing of the bleaching of the molecular cation. The belated bleaching of the $C_2H_4^+$ signal has already been observed by A. Ludwig and coworkers[9] who used a broad and energetic harmonic spectrum to ionize the molecule. For this reason they could neither identify the exact mechanism which leads to the observed delay nor the molecular state/geometry at which the interaction with the IR pulse can lead to H and H_2 loss. Here, by combining the selective excitation with the different harmonics and surface hopping calculations, we find an answer to these questions.

Figures 3(a)-(c) report the data of Fig. 2(c) (markers) together with the result of a fit based on exponentially-modified Gaussians (EMGs) (solid line). The width of the EMG is fixed to the cross-correlation width found in the related photoelectron calibration experiments, while the amplitude, zero position and decay rate are free parameters. In the case of H9 (Fig. 3(a)) the best fit is obtained with a sum of two signals, composed by 2 EMGs. The first signal is centered at $\tau = 0$ fs (cyan dotted curve in Fig. 3(a)) while the second (violet dotted curve in Fig. 3(a)) is a scaled copy of the former, delayed by 22.4 ± 1.9 fs. The first accounts for almost 74 % of the signal while the amplitude of the second for the remaining 26 %. The results obtained with H11 and H13 (Figs. 3(b),(c), respectively) are instead fitted with a single signal composed by 2 EMGs. In this case, a sinusoidal component has been added to the slow EMG in order to reproduce the oscillations which can be seen at positive delays. The fitting procedure reveals the bleaching to be centered at 19.8 ± 2.7 fs and 22.6 ± 1 fs for H11 and H13, respectively. The oscillation period is about 50 fs and seems to suggest a relevant role of the torsional motion when the initial excitation happens on the higher cationic states.[8] The observed timing of the molecular cation bleaching, instead, nicely relates to the timing of the non-radiative relaxation. Figures 3(d)-(f) display the calculated population on the first four cationic states (D0 to D3) after initial excitation by H9, H11 and H13 and following the prediction of Fig. 1(d). The thin curves are the populations convoluted by the experimental cross-correlation width of each harmonic. The

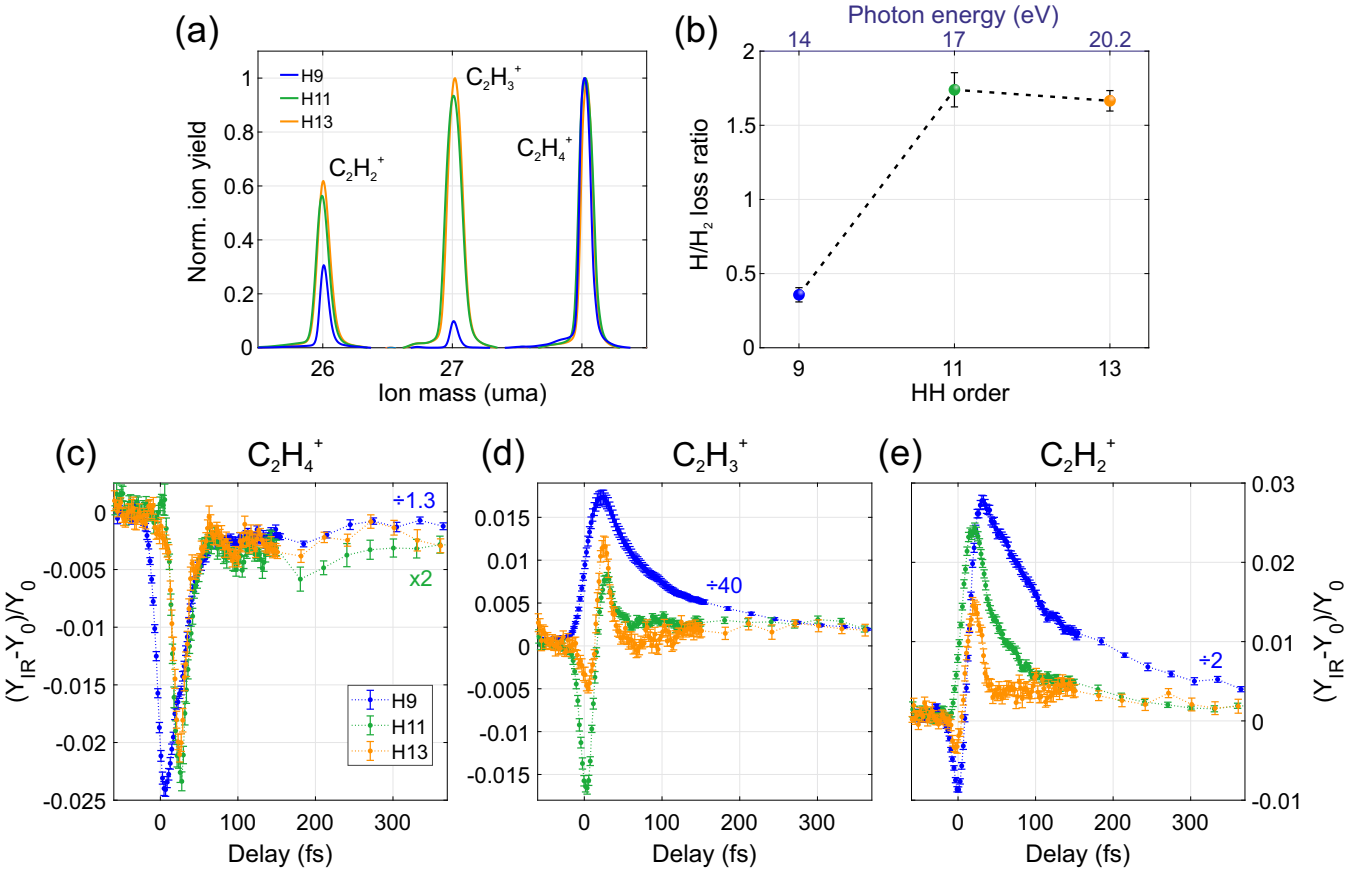

Figure 2: **(a)** Heavy fragment yields obtained with H9 (blue), H11 (green) and H13 (orange). While H13 and H11 give comparable fragment yields, H9 differs significantly. **(b)** H/H_2 loss ratio after excitation with the three different harmonics. **(c)** Differential $C_2H_4^+$ yield as a function of the delay between the XUV and IR pulse as obtained with the different harmonics. **(d)**, **(e)**, Same quantity but for the fragments $C_2H_3^+$ and $C_2H_2^+$, respectively.

vertical dashed red line marks the time at which the population on the ground state D0 exceeds that of the other states. As expected, the higher the initial photon energy, the longer it takes to the molecule to relax to D0. Nevertheless, most of the population has relaxed on D0 within 13 fs for H11 and 23 fs for H13. This confirms that the internal relaxation proceeds through ultrafast mechanisms,[10,19] and suggests a strong link to the belated $C_2H_4^+$ bleaching.

In order to further investigate the exact nature of the ultrafast relaxation we simulated dissociation yield up to 2 ps. The results, reported in Tab. 1, show a strong dependence on the initial excited state. The highest the initial state, the more kinetic energy the molecular wavepacket will have after relaxation and so the highest will be the dissociation yield (0 % for D0, 4 % for D1, 57 % for D2 and 69 % for D3). In particular, the states D2 and D3 lie 4 to 6 eV above D0 so that upon relaxation, the molecular wavepacket has enough energy to overcome the barrier for H dissociation,

Table 1: Simulated dissociation yield after 2 ps of dynamics starting from the states D0 to D3.

Initial state	Dissociation yield		
	$C_2H_4^+$	$C_2H_3^+$	$C_2H_2^+$
D0	100%	0%	0%
D1	96%	4%	1%
D2	43%	41%	16%
D3	31%	55%	13%

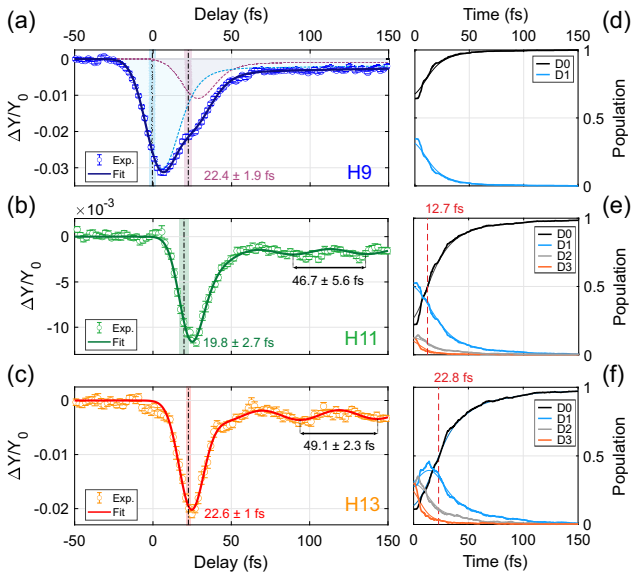

Figure 3: **(a)** Differential $C_2H_4^+$ yield after ionization with H9 (blue markers). The solid blue curve represents the result of a fitting procedure which accounts for two delayed components (highlighted by the cyan and violet dashed lines). **(b)**, **(c)**, Same quantity obtained with H11 and H13, respectively. In this case the data are fitted with a delayed bleaching and an oscillatory component. **(d)-(f)**, Calculated non-radiative relaxation of the first four cationic states after initial excitation by H9, H11 and H13, respectively.

which is about 2.7 eV[8] above the mean D0-D1 energy gap. This both explains the increased $C_2H_3^+$ and $C_2H_2^+$ production in the static spectra of Fig. 2(a), and offers an explanation for the pump-probe data of Fig. 3. After ionization with H9 the molecule is mostly left on the cation ground state, subsequent IR excitation can induce H and H_2 loss,[20] promptly bleaching the molecular cation signal at pump-probe overlap. With H11 and H13 the molecule is instead projected onto the excited states from which it takes a finite time to relax to D0 where the H and H_2 loss can be initiated by the IR pulse. For this reason, the $C_2H_4^+$ signal is delayed with respect to H9. The belated component observed in Fig. 3(a) at $\sim$ 22 fs originates from the fraction of excited states which are populated by H9. Indeed, the ratio D0 vs. excited states we can predict from the cross-sections[4] is about 65:35 and qualitative agrees with 74:26 extracted from the fit of the $C_2H_4^+$ differential yield.

Due to the energy spacing between the states, the IR excitation to D2 and D3 could happen by the absorption of 3 IR photons. We found that the excitation is dominated by a 3-IR-photon transition between D0 and D3 which is the only one displaying both a large portion of resonant wavepacket and transition dipole in the few fs after excitation (Fig. 4(a)).

Moreover, the simulations on D0 show that the D0-D3 transition dipole moment is the largest when the CC bond, r_{CC}, is elongated and the HCH angle, φ_{HCH}, is opened (see Fig. 4(c)). This explains why in the first 10 fs after excitation, when both r_{CC} and φ_{HCH} increase in phase (Fig. 4(b)), the D0-D3 transition dipole moment is the largest and more than 60 % of the wavepacket is 3-photon resonant. To be noted that the D0-D2 transition dipole moment also depends on the CC elongation, but the transition dipole moment is almost twice lower than for the transition D0-D3 in the first femtoseconds, indicating that the main photoexcited state is D3 (see SI). For pump-probe time delays longer than 50 fs, there is no clear variation of the experimental $C_2H_4^+$ yield, which could indicate that wavepacket has spread out or that exciting D2 or D3 outside the Franck-Condon region does not increase the dissociation yield.

The maximum excitation probability to D3, is observed for 1.45 Å$\leq$ r_{CC} $\leq$ 1.625 Å and 130° $\leq$ φ_{HCH} $\leq$ 145° (shaded gray rectangle in Fig. 4(c)). Figures 4(d)-(f) show the fraction of trajectories (black curve) that visits this particular geometry for different times after initial excitation on D1, D2 and D3, respectively. The nonradiative relaxation of the ethylene cation has been shown to occur either through a planar or twisted conical intersection (CI) between D0 and D1,[8] which is represented in figure 4(d)-(f) by respectively a dashed magenta and solid violet curve. The gray area shows the percentage of trajectories associated with the maximum excitation probability for initial excitation on D0. We observe that the higher the initial excitation, the later the molecule reaches the geome-

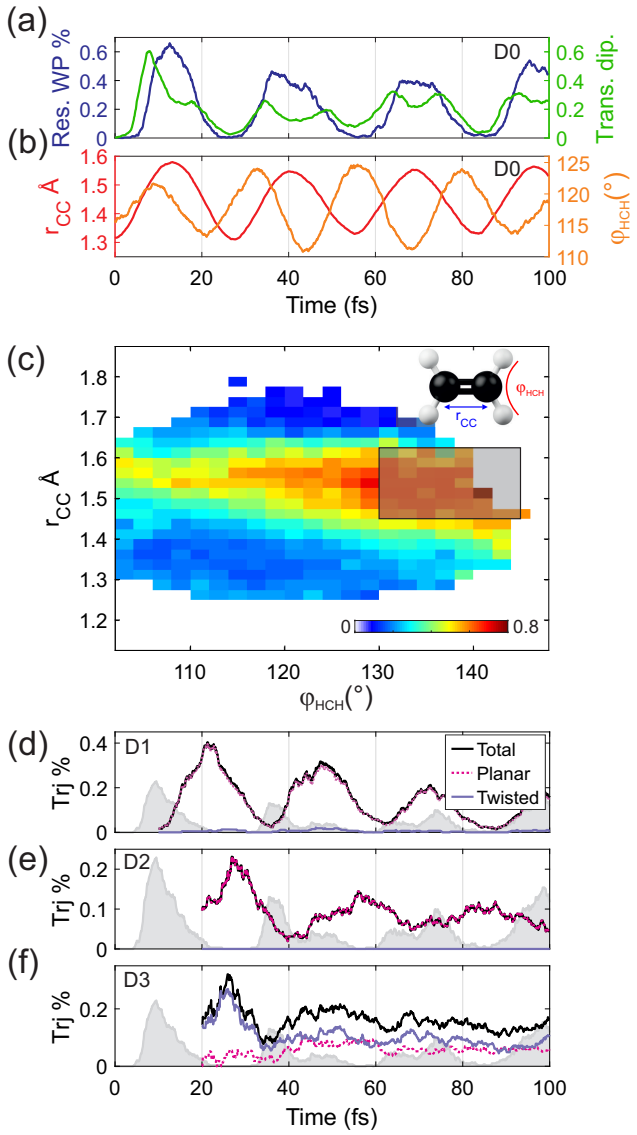

Figure 4: **(a)** Fraction of trajectories that are 3-IR-photon resonant between D0 and D3 (blue curve), together with the time evolution of the mean transition dipole moment between the same states (green curve). **(b)** Associated mean r_{CC} (red curve), and φ_{HCH} (orange curve). **(c)** D0-D3 transition dipole probability as a function of r_{CC} and φ_{HCH}. The black rectangle delimits the region where the transition probability is maximize (definition in the text). **(d)-(f)**, Percentage of trajectories falling into the black rectangle in (c) (solid black), calculated for initial excitation on D1, D2 and D3, respectively. The dashed magenta curve indicates the fraction of trajectories that have relaxed through a D0/D1 planar CI while in solid violet through a twisted D0/D1 CI. The gray area indicates the time evolution on D0.

try where it can be re-excited to D3, increasing fragmentation and thus decreasing the $C_2H_4^+$ yield. When compared to initial excitation on D0, excitation on D1 leads to a maximum number of trajectories in the correct geometry about 12 fs later, while for initial excitation on D2 and D3 this configuration is reached with a delay of about 18 fs. This is consistent with the data reported in Fig. 3, where the excitation with H11 and H13 produces a delayed $C_2H_4^+$ bleaching of about 20 fs. Moreover, the calculations allow to disclose the role of planar and twisted CIs in the ultrafast relaxation dynamics of the molecular cation. Indeed, while the wavepacket excited on D1 and D2 relaxes to the right geometry almost entirely through a planar CI (Figs. 4(d), (e)), excitation to D3 (Fig. 4(f)) relaxes both to planar and twisted CIs (almost equally divided between the two classes of CIs, in agreement with what observed in Ref.[8]), but only the trajectories coming from the twisted CI can be excited in the first 35 fs as the CC bond is elongated and the HCH angle open after the passage through the twisted CI, which enhances the photoexcitation yield. Therefore, while relaxation through planar CI would be slower, the higher internal energy on D3 allows the twisted CI seam to come into play, enabling fast relaxation and keeping the delay with D0 on a 20 fs-scale. The fact that a 25-fs delay has been observed also after excitation with higher photon energies[9] suggests that the twisted CI dominate the fast relaxation also when states higher than D3 are populated. Finally, Fig. 4(d)-(f) show clear oscillations, whose period is related to the twisting motion of the molecule and compares with the oscillations observed in Fig. 3 for excitation with H11 and H13. Every time the molecular wavepacket revisits the CI seams responsible for relaxation, a fraction of it reaches the correct geometry and re-excitation by the IR pulse can happen. The oscillation amplitude appears to be strongly reduced in the experimental data while it is overestimated in the calculations. This can be due to the limitations of the SH simulation. It is worth to notice that the oscillations in D1-D3 and D0 are almost out of phase. Therefore, if both the ground state and the excited states are populated, they are

expected to partially cancel each other. This explains why no oscillations are observed in the $C_2H_4^+$ yield obtained with H9 (Fig. 3(a)).

In summary, we presented a detailed study of the ultrafast relaxation dynamics that follow the photoionization of a prototype organic molecule like ethylene. Few-femtosecond EUV pulses produced with a TDCM are used to create different initial coherent populations of the first four cationic states. The subsequent relaxation dynamics are interviewed in a pump-probe fashion by a 15-fs IR pulse which further excites the molecule and induces H and H_2 loss. As a result, we observe a bleaching of the molecular cation signal, whose exact timing depends on the initially deposited energy. In particular, when the first excited states are populated, the bleaching peaks about 20 fs after ionization, while when the molecule is left in the ground state of $C_2H_4^+$, H and H_2 loss is maximum when IR and EUV pulses overlap in time. Detailed comparison with surface hopping excited state simulation allowed us to pinpoint the path followed by the molecule after excitation and demonstrate that the IR re-excitation proceeds through a resonant 3-photon absorption process between the cationic ground state and the third excited state. Moreover, we found the transition probability to correlate to the length of the CC bond and the aperture of the HCH angle. This allows us to prove that, while the ultrafast relaxation from the two lowest excited states is dominated by the planar CI, for higher excited states the twisted CI has a dominant role. Shedding a new light onto the ultrafast coupling between the internal degrees of freedom which mediate the ultrafast population transfer between the cationic states of a prototype molecule, our results move a step towards a precise optical control of molecular reactions on ultrafast time scales.

Acknowledgement We acknowledge useful scientific discussion with Prof. Horst Koeppel and Prof. Mike Robb. MN, ML, FF and LP acknowledge the contribution from the Italian Ministry for Research on "ELI Infrastructure - Italian RoadMap ESFRI", 2019. MN and ML further acknowledge funding from Laserlab-Europe EU-H2020 GA no. 871124. MN acknowledges funding from MIUR PRIN No. 20173B72NB. BM, CG and FR acknowledge support from the Fonds National de la Recherche, F.R.S.-FNRS, Belgium, #T.0132.16, and from the Consortium des Equipements de Calcul Intensif, CECI, #2.5020.11.

Supporting Information Available

The following files are available free of charge.

- SupportingInfo.pdf: Details on the experimental and computational methods, as well as extended experimental results

References

(1) Galbraith, M. C. E.; Scheit, S.; Golubev, N. V.; Reitsma, G.; Zhavoronkov, N.; Despré, V.; Lépine, F.; Kuleff, A. I.; Vrakking, M. J. J.; Kornilov, O. et al. Few-femtosecond passage of conical intersections in the benzene cation. *Nature Communications* **2017**, *8*, 1018.

(2) Nisoli, M.; Decleva, P.; Calegari, F.; Palacios, A.; Martín, F. Attosecond Electron Dynamics in Molecules. *Chemical Reviews* **2017**, *117*, 10760–10825.

(3) Borrego-Varillas, R.; Lucchini, M.; Nisoli, M. Attosecond spectroscopy for the investigation of ultrafast dynamics in atomic, molecular and solid-state physics. *Reports on Progress in Physics* **2022**, *85*, 066401.

(4) Berkowitz, J. *Atomic and Molecular Photoabsorption*; Elsevier: Amsterdam, 2015; pp 442–458.

(5) Tao, L.; Scrinzi, A. Photo-electron momentum spectra from minimal volumes: the time-dependent surface flux method. *New J. Phys.* **2012**, *14*, 013021.

(6) Allison, T. K.; Tao, H.; Glover, W. J.; Wright, T. W.; Stooke, A. M.; Khurmi, C.; van Tilborg, J.; Liu, Y.; Falcone, R. W.; Martínez, T. J. et al. Ultrafast internal conversion in ethylene. II. Mechanisms and pathways for quenching and hydrogen elimination. *The Journal of Chemical Physics* **2012**, *136*, 124317.

(7) Femtosecond isomerization dynamics in the ethylene cation measured in an EUV-pump NIR-probe configuration. *Journal of Physics B: Atomic, Molecular and Optical Physics* **2009**, *42*, 081002.

(8) Joalland, B.; Mori, T.; Martínez, T. J.; Suits, A. G. Photochemical Dynamics of Ethylene Cation $C_2H_4^+$. *The Journal of Physical Chemistry Letters* **2014**, *5*, 1467–1471.

(9) Ludwig, A.; Liberatore, E.; Herrmann, J.; Kasmi, L.; López-Tarifa, P.; Gallmann, L.; Rothlisberger, U.; Keller, U.; Lucchini, M. Ultrafast Relaxation Dynamics of the Ethylene Cation $C_2H_4^+$. *The Journal of Physical Chemistry Letters* **2016**, *7*, 1901–1906, PMID: 27139223.

(10) Zinchenko, K. S.; Ardana-Lamas, F.; Seidu, I.; Neville, S. P.; van der Veen, J.; Lanfaloni, V. U.; Schuurman, M. S.; Wörner, H. J. Sub-7-femtosecond conical-intersection dynamics probed at the carbon K-edge. *Science* **2021**, *371*, 489–494.

(11) Sannen, C.; Raşeev, G.; Galloy, C.; Fauville, G.; Lorquet, J. C. Unimolecular decay paths of electronically excited species. II. The $C_2H_4^+$ ion. *The Journal of Chemical Physics* **1981**, *74*, 2402–2411.

(12) Mignolet, B.; Curchod, B. F. E.; Martínez, T. J. Rich Athermal Ground-State Chemistry Triggered by Dynamics through a Conical Intersection. *Angewandte Chemie* **2016**, *128*, 15217–15220.

(13) Richter, M.; Marquetand, P.; González-Vázquez, J.; Sola, I.; González, L. SHARC: *ab Initio* Molecular Dynamics with Surface Hopping in the Adiabatic Representation Including Arbitrary Couplings. *Journal of Chemical Theory and Computation* **2011**, *7*, 1253–1258.

(14) Poletto, L.; Villoresi, P.; Frassetto, F.; Calegari, F.; Ferrari, F.; Lucchini, M.; Sansone, G.; Nisoli, M. Time-delay compensated monochromator for the spectral selection of extreme-ultraviolet high-order laser harmonics. *Review of Scientific Instruments* **2009**, *80*, 123109.

(15) Lucchini, M.; Lucarelli, G. D.; Murari, M.; Trabattoni, A.; Fabris, N.; Frassetto, F.; Silvestri, S. D.; Poletto, L.; Nisoli, M. Few-femtosecond extreme-ultraviolet pulses fully reconstructed by a ptychographic technique. *Opt. Express* **2018**, *26*, 6771–6784.

(16) Mackie, R. A.; Scully, S. W. J.; Sands, A. M.; Browning, R.; Dunn, K. F.; Latimer, C. J. A photoionization mass spectrometric study of acetylene and ethylene in the VUV spectral region. *Int. J. Mass Spectrom.* **2003**, *223-224*, 67–79.

(17) Holland, D.; Shaw, D.; Hayes, M.; Shpinkova, L.; Rennie, E.; Karlsson, L.; Baltzer, P.; Wannberg, B. A photoabsorption, photodissociation and photoelectron spectroscopy study of C2H4 and C2D4. *Chemical Physics* **1997**, *219*, 91 – 116.

(18) Moio, B.; Dolso, G. L.; Inzani, G.; Di Palo, N.; Borrego-Varillas, R.; Nisoli, M.; Lucchini, M. Time-frequency mapping of two-colour photoemission driven by harmonic radiation. *Journal of Physics B: Atomic, Molecular and Optical Physics* **2021**, *54*, 154003.

(19) Köppel, H.; Domcke, W.; Cederbaum, L. Multimode molecular dynamics approximation beyond the Born-Oppenheimer. *Adv. Chem. Phys.* **1984**, *57*, 59.

(20) Stockbauer, R.; Inghram, M. G. Threshold photoelectron-photoion coincidence mass spectrometric study of ethylene and

ethylene-d4. *The Journal of Chemical Physics* **1975**, *62*, 4862–4870.